

Sol–Gel-Derived TiO₂ and TiO₂/Cu Nanoparticles: Synthesis, Characterization, and Antibacterial Efficacy

Njabulo Sondezi, Zikhona Njengele-Tetyana, Kgabo Phillemon Matabola, and Thollwana Andretta Makhetha*



Cite This: *ACS Omega* 2024, 9, 15959–15970



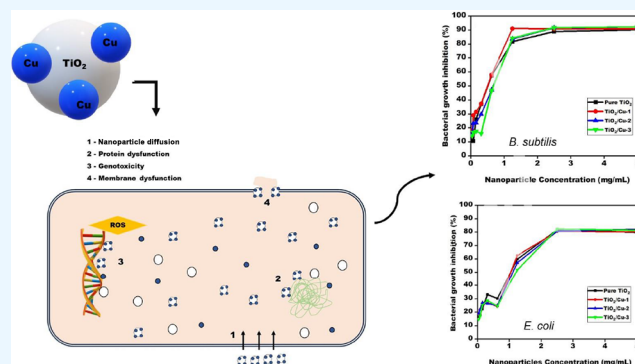
Read Online

ACCESS |

Metrics & More

Article Recommendations

ABSTRACT: This study reports on the antibacterial efficacy of both the TiO₂ and TiO₂/Cu nanoparticles prepared through the sol–gel method. The materials were characterized by scanning electron microscopy (SEM), transmission electron microscopy (TEM), energy-dispersive X-ray spectroscopy (EDS), X-ray diffraction (XRD), Fourier-transform infrared spectroscopy (FTIR), Raman spectroscopy, X-ray photoelectron spectroscopy (XPS), thermogravimetric analysis (TGA), and Brunauer–Emmett–Teller (BET) analysis. The SEM and TEM showed the spherical morphology of the nanoparticles, while EDX and XPS confirmed the incorporation of Cu into the TiO₂ nanoparticles. The XRD confirmed the formation of the tetragonal anatase phase of TiO₂/Cu while the FTIR revealed the functional groups linked to the doped TiO₂ nanoparticles. The thermal stability of TiO₂/Cu was found to be lower than pure TiO₂. Moreover, TiO₂ and the doped TiO₂ nanoparticles were notably effective against *Bacillus subtilis* (*B. subtilis*) and *Escherichia coli* (*E. coli*); however, the addition of Cu to TiO₂ did not have any effect on the antibacterial activity probably due to the lower weight content in the composites. Interestingly, the antibacterial efficiency was determined to be 90 and 80% against *B. subtilis* and *E. coli*, respectively.



1. INTRODUCTION

Water is a vital aspect of life and is required in industrial, agricultural, and domestic domains. The emitted toxic pollutants into the water bodies cause serious concerns.¹ Bacterial pathogens (*Escherichia coli*) and heavy metals (Pb, Cd, and Zn), which are dangerous to humans, are among the primary contaminants of concern.² Thus, there is a necessity to develop and synthesize smart materials capable of eliminating such pollutants from water.³ With the advent of nanotechnology, nanomaterials emerged as the potential solution to removing waterborne contaminants precisely due to their various shapes and sizes (1 to 100 nm), enormous surface area, and strong reactivity. As such, they have found applications in different fields such as healthcare, sensors, energy storage/generation, and drinking water purification.^{1,4,5}

Among different materials, metal oxides (MOs) have been intensively investigated for a variety of uses such as renewable energy, medicine, sensors, and photocatalysts.^{3,5} They demonstrated distinct optical, electronic, physical, and chemical characteristics in comparison to those of their bulk form. The use of MOs relies on the characteristics like antibacterial, photocatalytic, conductivity, crystalline structure, stability, larger surface area, morphology, and size.^{6,7} A variety of studies have been conducted with a view of enhancing the

efficiency of these transition MOs. These were done through doping the MOs with other nanomaterials including metals, metal oxides, and carbon nanoparticles, which were found to be beneficial for several new applications in material science, biology, physics, and chemistry.⁵ Following alteration, the transition MO-based nanoparticles possessed novel features such as increased porosity, surface area, and improved surface functionalities.⁵ Some of the most commonly explored MO nanoparticles are copper oxide (CuO), silver oxide (Ag₂O), magnesium oxide (MgO), zinc oxide (ZnO), iron oxide (Fe₂O₃), and titanium dioxide (TiO₂).^{8,9}

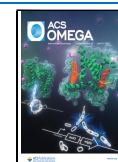
Among these MO nanoparticles, TiO₂ is the most explored nanomaterial due to its excellent physicochemical, mechanical stability, earth abundance, and antibacterial properties.^{10,11–13} Furthermore, TiO₂ turned out to have strong capabilities as an adsorbent material for the removal of heavy metal ions in water.^{14,16} In addition, the antibacterial effect of these TiO₂

Received: November 22, 2023

Revised: January 7, 2024

Accepted: March 5, 2024

Published: March 29, 2024



nanoparticles is attributed to reactive oxygen species (ROS) mediated membrane degradation.^{14,15,17} The nanoparticles can react with O₂ and –OH functional groups attached to the surface to produce free radicals. As a result, the enhanced surface area and small size can improve the antibacterial effect as the nanoparticles can easily pass through the membrane and kill the bacteria.¹⁸ Although TiO₂ nanoparticles do possess antibacterial properties, there are some limitations affecting their full potential, particularly under dark conditions. To mitigate this, TiO₂ is doped with metals such as copper (Cu), palladium (Pd), and silver (Ag), which were discovered to be capable of enhancing the antibacterial properties.¹⁹ Of all these metals, Cu turned out to be an excellent choice for enhancing antibacterial properties of TiO₂ because it is an essential element for living organisms and very affordable as compared to the other dopants.²⁰ The antibacterial action of Cu is accomplished through destroying the bacterial cell membranes.²¹ Chen et al. reported that, in dark conditions, the synergistic antibacterial properties of TiO₂/Cu are responsible for the enhanced antibacterial effects, which depends on the production of reactive oxygen species that disintegrates the bacterial cell membrane by lipid peroxidation.²²

This work provides new insights into lower temperature pure TiO₂ and TiO₂/Cu nanoparticles with varied amounts of copper synthesized by using a sol–gel method. In most cases, high calcination temperatures and high concentrations of Cu were used to make Cu-doped TiO₂ for antibacterial activities. Furthermore, the synthesized materials proved to be effective under dark conditions, wherein, similar materials reported no activity as shown in Table 1, while others used light source such as UV light for antibacterial activity.²³

Table 1. Comparison of the Antibacterial Performance of the Nanoparticles Without a Light Source Such as UV or Visible Light

nanoparticles	bacteria	antibacterial efficiency	reference
TiO ₂ /Cu	<i>S. aureus</i>	no activity	Fuentes, 2021 ²⁴
TiO ₂ /Cu	<i>S. aureus</i> , <i>E. coli</i>	no activity	Mathew, 2018 ²⁵
TiO ₂ /Cu	<i>S. aureus</i> , <i>E. coli</i>	no activity	Sagadevan, 2020 ²⁶
TiO ₂ /Cu	<i>B. subtilis</i> , <i>E. coli</i>	90%, 80%	current study

In this study, pure TiO₂ and TiO₂/Cu nanoparticles with varied amounts of copper were synthesized using a sol–gel method.⁶ The synthesized samples were characterized utilizing a variety of techniques such as SEM, TEM, EDX, XRD, FTIR, Raman Spectroscopy, XPS, TGA, and BET. Moreover, the level of their antibacterial efficiency was tested in the dark against two bacterial strains, namely, *Bacillus subtilis* (*B. subtilis*) and *Escherichia coli* (*E. coli*).

2. MATERIALS AND METHODS

2.1. Materials. Titanium isopropoxide (TTIP, 27.8–28.6% TiO₂, SRLchem, India), copper(II) nitrate trihydrate (Cu(NO₃)₂·0.3 H₂O, 98.0–103%, Sigma-Aldrich, Spain), glacial acetic acid (99.9%, SRLchem, India), and 2-propanol (99.9%, Honeywell, France) were used. All of the reagents were used as received from the supplier.

2.2. Synthesis of TiO₂ and TiO₂/Cu Nanoparticles. The nanoparticles were synthesized through the sol–gel method as reported in the literature.^{27,28}

2.2.1. Synthesis of TiO₂. First, TTIP (2.5 mL) was added dropwise to the mixture of 2-propanol (10 mL) and glacial acetic acid (3 mL) under stirring for 30 min. After stirring, a white solution was formed, and distilled water (2 mL) was added to form a white gel. The latter was dried in an oven at 100 °C for 2 h followed by calcination at 350 °C for 3 h.

2.2.2. Synthesis of TiO₂/Cu Nanoparticles. Cu(NO₃)₂·3H₂O was dissolved in distilled water (10 mL) to prepare copper solutions (0.5, 1, and 2 wt %) as shown in Table 2. The

Table 2. Ratio of Components Used for the Preparation of TiO₂/Cu Composites

labels	moles of TiO ₂ (mmol)	moles of Cu (mmol)
Pure TiO ₂	8.6200	0
TiO ₂ /Cu-1	8.6200	0.2069
TiO ₂ /Cu-2	8.6200	0.4139
TiO ₂ /Cu-3	8.6200	0.8278

latter solutions and the TiO₂ solution prepared in section 2.2.1 were mixed under stirring at a temperature of 80 °C until a blue gel was obtained. The gel was then dried in an oven at 100 °C for 2 h followed by calcination at 350 °C for 3 h to form TiO₂ doped with different concentrations of Cu. As compared to the previously reported methods, only the calcination temperature was changed to 350 °C to result in an anatase phase with a small particle size, which is suitable for intended application.

2.3. Characterizations of TiO₂ and TiO₂/Cu Nanoparticles. Morphological changes were investigated using scanning electron microscopy (SEM) using VEGA3 TESCAN (Czech Republic) at an accelerated voltage of 20 kV. The samples were carbon-coated prior to analysis. Transmission electron microscope (TEM) analyses were performed using a JEOL-JEM-2010 (Japan) operated at an accelerating voltage of 200 kV. The elemental composition of the samples was studied using the energy dispersive X-ray spectrometer (EDS) (Oxford Instruments) and X-ray photoelectron spectroscopy (XPS) (KRATOS-SUPRA). Powder X-ray diffraction (p-XRD; PANalytical X'Pert Pro-powder diffractometer, Eindhoven, Netherlands) was used to determine the crystalline structures of the materials. Raman spectra were obtained using Thermo Scientific DXR2 Smart Raman (USA) at a Raman shift ranging from 100 to 3500 cm⁻¹. Fourier-transform infrared spectroscopy (FTIR), PerkinElmer Spectrum 100 (German) was employed to probe the change in chemical composition. The spectra were recorded in the wavelength range from 400 to 4000 cm⁻¹. Thermogravimetric analysis STA7200RV (Hitachi) was performed by heating the samples from 30 to 800 °C at a scanning rate of 10 °C/min under a nitrogen (N₂) atmosphere with a flow rate of 50 mL/min. Brunauer–Emmett–Teller (BET) (Tristar II, micromeritics, USA) was used to examine the surface of the samples at 150 °C.

2.4. Antibacterial Studies. **2.4.1. Bacterial Strains and Culture Conditions.** The antibacterial efficacy of pure TiO₂ and TiO₂/Cu nanoparticles were tested against two bacterial strains, namely *Bacillus subtilis* (*B. subtilis*) and *Escherichia coli* (*E. coli*). The microorganisms were first cultured on nutrient agar plates at 37 °C overnight (~16 h), and suspension cultures were obtained by picking single colonies of the organisms from the agar plates and inoculating them in nutrient broth. The samples were allowed to grow for another 16 h at 37 °C in an orbital shaker (150 rpm).

2.4.2. Antimicrobial Activity Testing. **2.4.2.1. MIC Determination.** The minimum inhibitory concentrations (MICs) of the nanoparticles were determined using the broth microdilution method defined by the Clinical and Laboratory Standards Institute²⁹ in sterile 96-well microtiter plates. Briefly, the test strains were precultured at 37 °C overnight, and the concentrations were adjusted to $\sim 1.5 \times 10^8$ CFU/mL, turbidity that is equivalent to the 0.5 McFarland standard, in nutrient broth prior to use. 2-fold serial dilutions of the nanoparticles, ranging from 10 to 0.078 mg/mL, were added to the 96-well plates at 100 μ L followed by 100 μ L of the diluted bacterial cultures, resulting in the following final nanoparticle concentrations: 5, 2.5, 1.5, 0.625, 0.312, 0.156, 0.078, and 0.039 mg/mL. Ampicillin (0.5–0.0039 mg/mL) and Gentamicin (0.05–0.0039 mg/mL) were used as positive controls against *E. coli* and *B. subtilis*, respectively, while bacterial cells treated with 2% DMSO in nutrient broth (without any nanoparticles) served as negative controls. The plates were covered and incubated at 37 °C overnight.

Following the incubation period, 40 μ L of p-Iodonitrotrazolium chloride dye (INT; Sigma), at a concentration of 0.2 mg/mL in water, was added to each well, and the plates were incubated at 37 °C for an additional 30 min.³⁰ Viable bacteria reduce the pale-yellow dye to a pink/purple colored product. MIC values were taken as the minimum concentration of nanoparticles at which there was no pink/purple color development, which denotes complete inhibition of bacterial growth. The observations were further validated by measuring the absorbance of the plates at 490 nm using a spectrophotometer (Molecular Devices). The data were normalized, and the MIC₅₀ values, defined as the lowest compound concentration that reduces bacterial growth by 50%, were determined using GraphPad Prism software.

The percentage of bacterial growth inhibition attained at different concentrations of the test samples was calculated by using the following equation:

$$\begin{aligned} & \% \text{Bacterial Growth Inhibition} \\ &= 1 - \left(\frac{\text{Absorbance of Sample}}{\text{Absorbance of Control}} \right) \times 100 \end{aligned} \quad (1)$$

2.4.2.2. MBC Determination. The bactericidal activity of the nanomaterials against the test bacterial strains was investigated by determining their minimum bactericidal concentrations (MBCs). For this assay, 50 μ L of the samples, which did not show any visible bacterial growth after incubations in the MIC assay, were transferred onto fresh nutrient agar plates and incubated at 37 °C overnight. MBC is defined as the lowest concentration at which there was no bacterial growth observed on the plates.

3. RESULTS AND DISCUSSION

3.1. Scanning Electron Microscopy (SEM) Analysis. Figure 1 demonstrates the SEM images of the prepared TiO₂ and TiO₂/Cu nanoparticles with different loadings of Cu nanoparticles. The pure TiO₂ nanoparticles (Figure 1a) show irregular differently shaped particles appearing to be made up of several fused nanospheres. This observation could be caused by calcination, which resulted into agglomeration.³¹ The latter occurred due to high surface energy, surface area, surface tension, attraction among the NPs, and oxidation of NPs. It is further observed in Figure 1b–d that with the increase in Cu loading, the size of the irregular shaped particles is seen to be

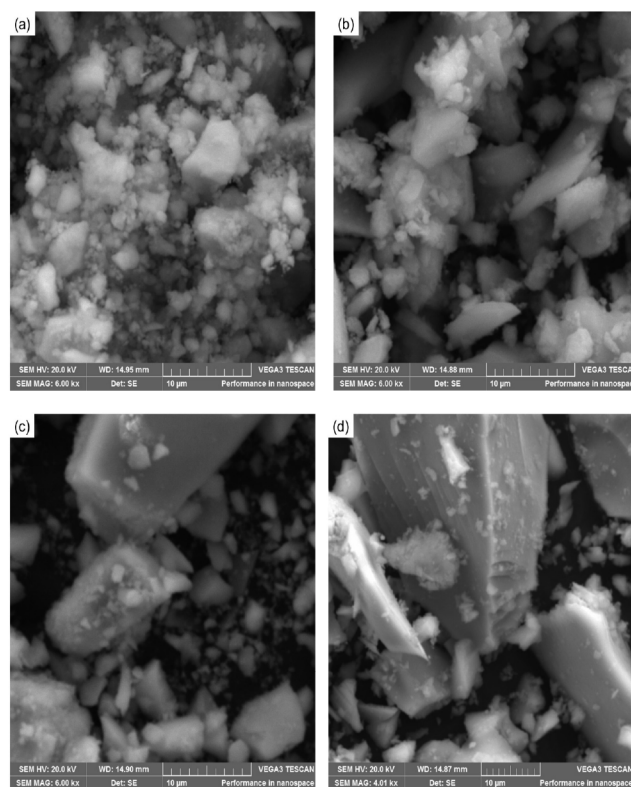


Figure 1. SEM images of (a) pure TiO₂, (b) TiO₂/Cu-1, (c) TiO₂/Cu-2, and (d) TiO₂/Cu-3 nanoparticles.

increasing while agglomeration is decreased. Therefore, a decrease in agglomeration (uniformly distributed nanoparticles) caused by decreased interparticle forces may result in higher surface area and high antibacterial activity.³² Moreover, it is also noticed that the doped TiO₂ (Figure 1b–d) nanoparticles seem to be less rough compared to the pure TiO₂ nanoparticles. The surface roughness of the nanoparticles can impact the antibacterial properties by enhancing bacterial attachment and cell membrane disruption. These rough surfaces provide more sites for bacterial attachment, increasing likelihood of antibacterial effects through physical and chemical interactions. Additionally, roughness may enhance the efficacy of nanoparticles in penetrating bacterial cell membranes, resulting in improved antibacterial outcomes.

3.2. Transmission Electron Microscopy (TEM) Analysis. Figure 2 presents the TEM images and size distribution curves of TiO₂ and TiO₂/Cu nanoparticles with different loadings of the Cu nanoparticles. It is seen that particles are generated during the synthesis method through condensation and hydrolysis reactions of the solvents and the precursors. Agglomeration is formed when particles adhere to each other due to weak forces resulting in the formation of clusters (Figure 2a).³³ It has been established that synthesized TiO₂ and TiO₂/Cu nanoparticles (Figure 2a–d) have an agglomerated spherical shape morphology that is linked to condensation reactions that occurred at particle interactions during the calcination process. These results seem to compare well with the SEM images in Figure 1 with respect to agglomeration. The size distribution for pure TiO₂ was found to be 10.035 nm, while TiO₂/Cu-1, TiO₂/Cu-2, and TiO₂/Cu-3 had the average particle size of 9.370, 8.842, and 8.878 nm,

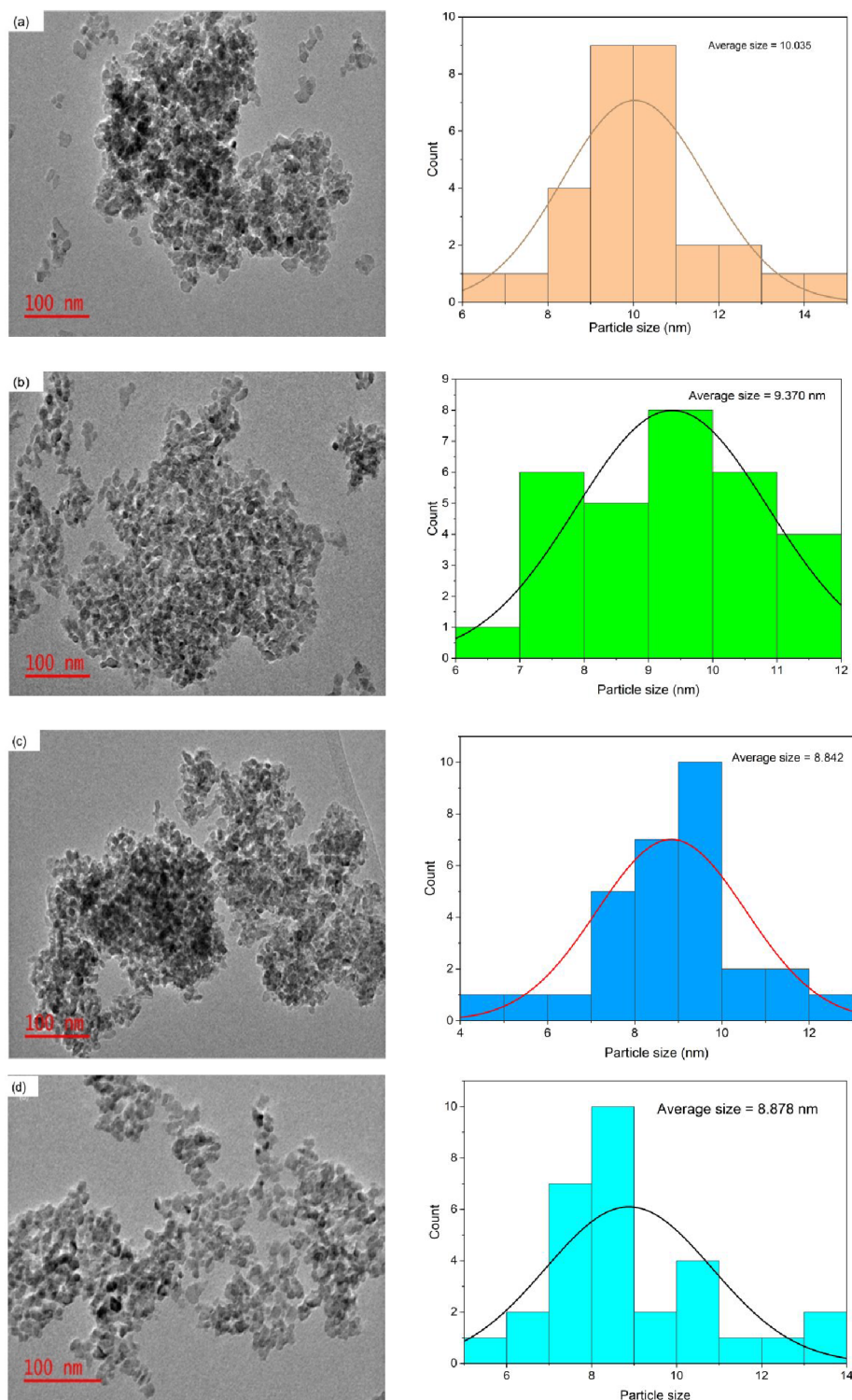


Figure 2. TEM images and size distribution curves of (a) pure TiO₂, (b) TiO₂/Cu-1, (c) TiO₂/Cu-2, and (d) TiO₂/Cu-3 nanoparticles.

respectively. When compared with previous works,^{27,28} the synthesized TiO₂ and TiO₂/Cu nanoparticles in this study had smaller particle sizes which could be beneficial for antibacterial applications. Whereas, Yadal et al.²⁸ reported that there was no antibacterial activity for TiO₂/Cu against Gram-positive (*S. Aureus*) and Gram-negative (*E. coli*). The total surface area-to-volume proportion for nanoparticles rises as their size decreases, hence, could improve the effectiveness of antibacterial agents.³⁴ Anitha and Khadar³⁵ observed that the

reduction in size was an indication of Cu ion incorporation in the TiO₂ lattice, which caused TiO₂ growth restrictions due to an increasing amount of Cu atoms near the Ti atom growth sites. The same trend was observed in this study; however, a slight increase in size was observed at TiO₂/Cu-3 probably due to more Cu nanoparticles.

3.3. Energy-Dispersive X-Ray Spectroscopy (EDX) Analysis. Figure 3 exhibits the EDS spectra of both TiO₂ (Figure 3a) and TiO₂/Cu (Figure 3b–d) nanoparticles. The

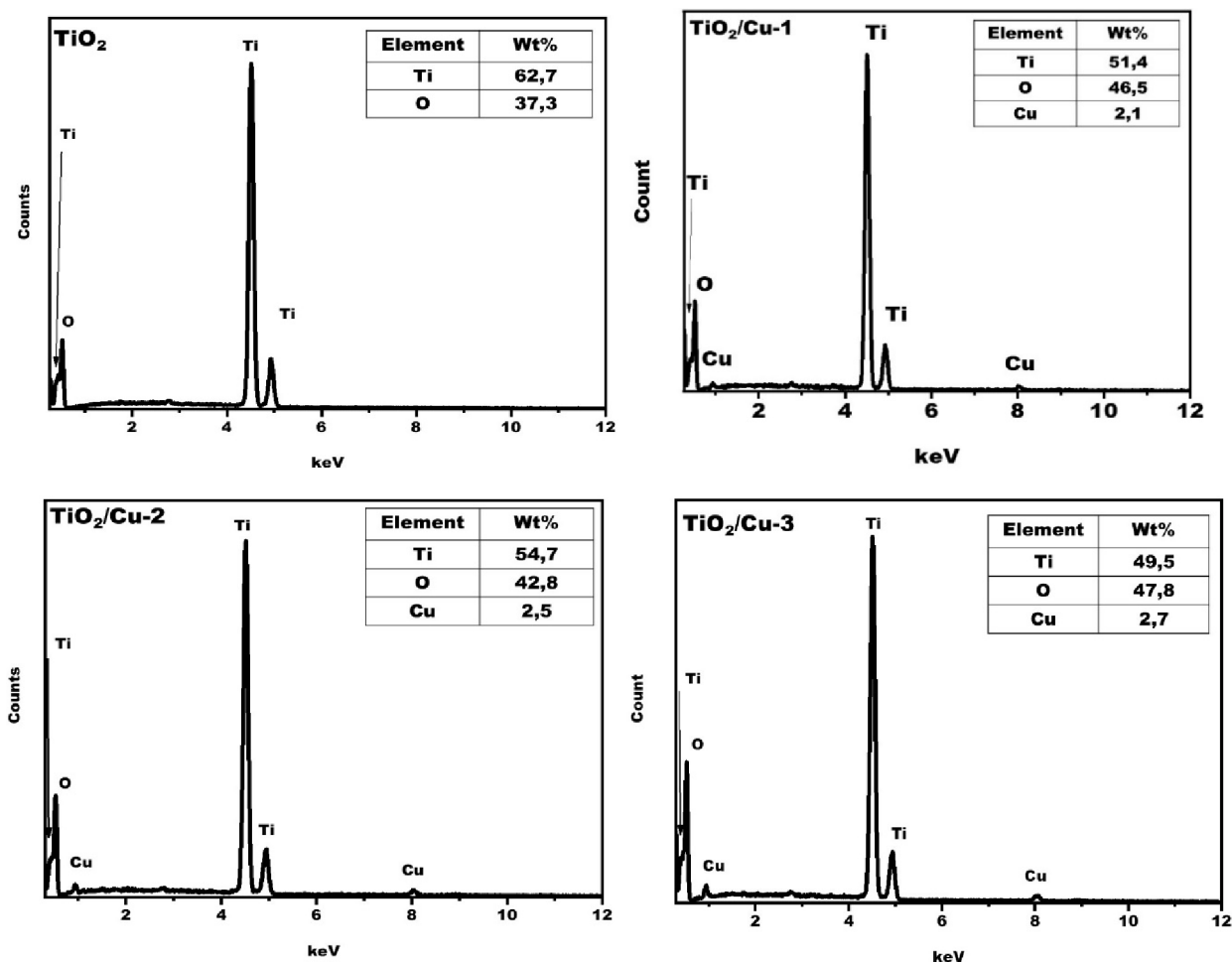


Figure 3. EDX spectra of TiO_2 and TiO_2/Cu nanoparticles.

EDS spectrum for the pure TiO_2 nanoparticles (Figure 3a) consists of only Ti and O while the spectra for the TiO_2/Cu nanoparticles show the presence of Ti, O, and Cu (Figure 3b–d). The presence of Cu in doped TiO_2 confirms the successful formation of Cu-doped TiO_2 nanoparticles. As expected, the atomic % of Cu increases with an increase in Cu loading in TiO_2/Cu . The Cu atomic % were found to be 2.1%, 2.5%, and 2.7% for TiO_2/Cu -1, TiO_2/Cu -2, and TiO_2/Cu -3, respectively. However, the amounts of Ti atoms were lower in the TiO_2/Cu nanoparticles as compared to pure TiO_2 while the O atoms were higher in TiO_2/Cu in comparison to TiO_2 . Pal et al.³⁶ observed the same trend. The elemental mapping (Figure 4a–b) demonstrates that the Cu atoms are uniformly dispersed on the TiO_2 surface for all the TiO_2/Cu samples. Ahmadiasl et al.³⁷ who confirmed the homogeneous distribution of Cu in the Cu-doped TiO_2 nanoparticles have reported similar results.

3.4. X-Ray Photoelectron Spectroscopy (XPS) Analysis. The XPS analysis was further utilized to examine the elemental components and atomic states of both TiO_2 and TiO_2/Cu nanoparticles. The XPS survey scan is presented in Figure 5a while the high-resolution spectra of TiO_2 , TiO_2/Cu -1, TiO_2/Cu -2, and TiO_2/Cu -3 are shown in Figures 5b–e, respectively. It can be noticed from the XPS survey spectra (Figure 5a) that major elements of C 1s, Ti 2p, O 1s, and Cu 2p are shown which are ascribed to both the TiO_2 and TiO_2/Cu nanoparticles.

Figure 5b (TiO_2) indicates XPS spectra of Ti 2p with two clear peaks at 458.2 and 464 binding energies (eV) corresponding to Ti 2p_{1/2} and Ti 2p_{3/2}, respectively. The literature has indicated that the difference in eV varied by about 5.8 eV is because of the spin orbit split.^{36,39} The O 1s spectra (Figure 5b, TiO_2) exhibited three deconvoluted peaks at 529.5, 531.3, and 532.7 eV, attributed to metal oxide, C–O and C=O, respectively. As for the TiO_2/Cu –1 nanoparticles (Figure 5c), the Ti 2p spectra showed two deconvoluted peaks at 458.2 and 463.8 eV corresponding to Ti 2p_{1/2} and Ti 2p_{3/2}, respectively. Meanwhile, the O 1s had peaks at 531.5 and 533 due to the presence of O 1s (metal oxide), O 1s (C–O), and the presence of O 1s (C=O), respectively. Moreover, the Cu 2p peak was observed at 931.6 eV indicating the successful formation of the TiO_2/Cu -1 nanoparticles. Figure 5d (TiO_2/Cu -2) and 5e (TiO_2/Cu -3) display the Ti 2p and O 1s spectra indicating the formation of the TiO_2 nanoparticles. Interestingly, both TiO_2/Cu -2 and TiO_2/Cu -3 nanoparticles showed Cu 2p spectra with peaks at 931.9 and 932.6 eV, respectively. As a result, the presence of the Cu metal through XPS analysis confirmed the formation of the TiO_2/Cu nanoparticles. These results are in agreement with the earlier-described EDS analysis.

3.5. X-Ray Diffraction (XRD) Analysis. X-ray diffraction (XRD) was employed to determine the phases, crystallographic plane structures, and crystalline sizes of the prepared nanoparticles. The XRD patterns of TiO_2 and Cu-doped TiO_2

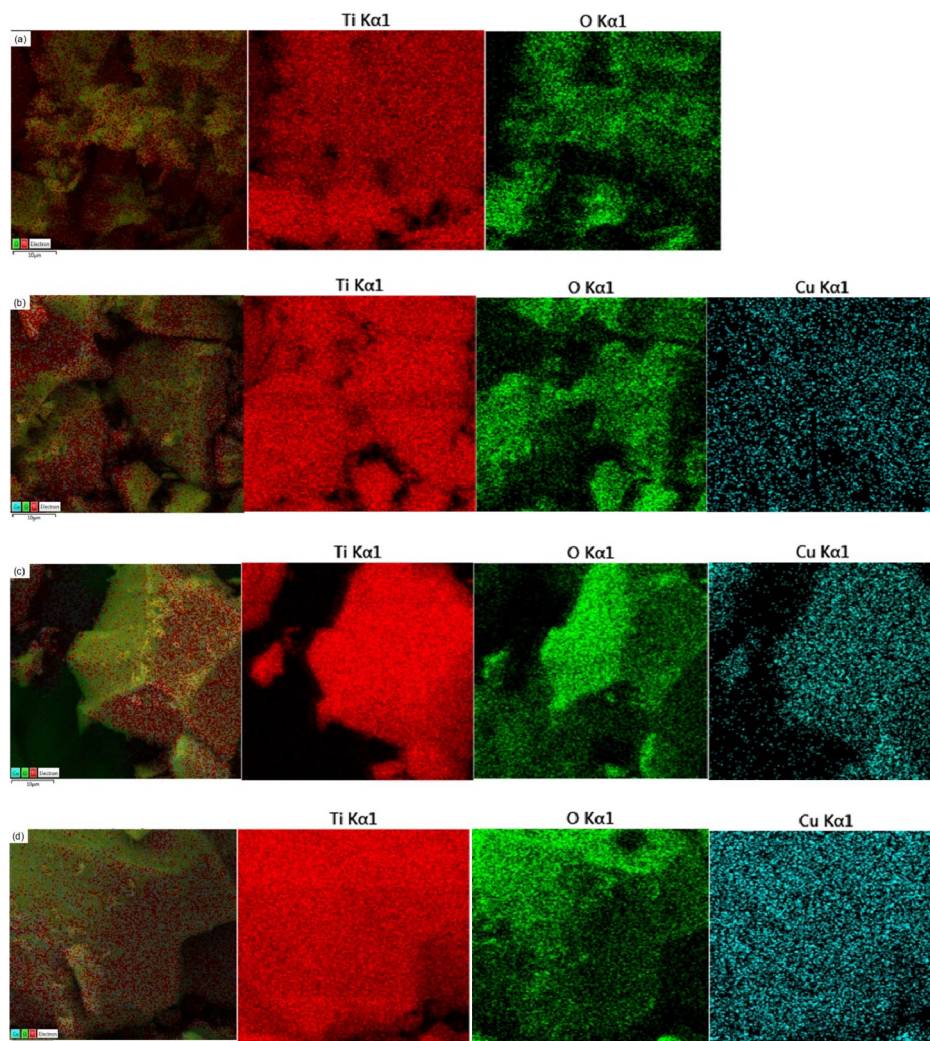


Figure 4. EDS mapping of (a) TiO_2 , (b) $\text{TiO}_2/\text{Cu-1}$, (c) $\text{TiO}_2/\text{Cu-2}$, and (d) $\text{TiO}_2/\text{Cu-3}$ nanoparticles.

are shown in Figure 6. The absorption bands at $2\theta = 25^\circ, 37^\circ, 47^\circ, 54^\circ, 55^\circ, 63^\circ, 69^\circ, 70^\circ,$ and 75° correspond to the plane indices (101), (004), (200), (105), (211), (204), (116), (220), and (215), respectively. These planes belong to the tetragonal anatase phase of TiO_2/Cu that correlates with the standard spectrum (JCPDS card 21-1272). The XRD spectra of the doped TiO_2 nanoparticles had no extra peaks of dopant or any crystal phase of the dopant species. This phenomenon does not guarantee that Cu-based planes and/or phases are not absent in the doped TiO_2 . This might mean that the Cu metals are evenly distributed within anatase crystallites in the shape of small clusters. As a result, diffraction arising from the TiO_2 surface might be more intense as compared to diffraction from Cu. However, the peak intensities of the $\text{TiO}_2/\text{Cu-1}$ and $\text{TiO}_2/\text{Cu-2}$ nanoparticles are higher as compared to the pure TiO_2 and the $\text{TiO}_2/\text{Cu-3}$ nanoparticles. This increased intensity suggests the successful incorporation of Cu onto the TiO_2 surface.²⁸ The grain size of the nanoparticles decreased as the Cu content increased as determined by Scherrer's equation (eq 2). The calculated particle sizes were determined to be 9.774, 8.197, 7.688, and 8.324 nm for pure TiO_2 , $\text{TiO}_2/\text{Cu-1}$, $\text{TiO}_2/\text{Cu-2}$, and $\text{TiO}_2/\text{Cu-3}$, respectively. However, a slight increase in particle size was observed in $\text{TiO}_2/\text{Cu-3}$. These results compare quite well with the TEM data.

$$D = \frac{0.9\lambda}{\beta \cos \theta} \quad (2)$$

3.6. Raman Spectroscopy Analysis. Raman spectroscopy was used to analyze the alteration in structure of TiO_2 caused by the incorporation of dopant ions. Figure 7 shows the Raman spectra of both the TiO_2 and TiO_2/Cu nanoparticles with different loadings of Cu. The TiO_2/Cu spectra showed no secondary peaks that can be associated with Cu or Cu-oxides, and this observation is consistent with the XRD analysis data.³⁸ The absence of the Cu peaks does not constitute the absence of Cu within the composite as the SEM-EDX, mapping as well as the XPS analysis confirmed the presence of Cu in the composites. Peaks at 152 and 643 cm^{-1} correspond to the E_g mode while the peak at 400 cm^{-1} corresponds to B_{1g} , and the one at 529 cm^{-1} corresponds to $\text{A}_{1g} + \text{B}_{1g}$ modes.³⁵ Raguram and Rajni³³ stated that the symmetric stretching vibrations of O–Ti–O in TiO_2 are responsible for the E_g and B_{1g} peaks which results from symmetric bending vibration of O–Ti–O, while A_{1g} are from the asymmetric bending vibrations. The introduction of Cu onto the TiO_2 surface resulted in a decrease in intensity of the peaks which demonstrated the substitution of Cu^{2+} ions at Ti^{4+} , thus altering the crystal properties as well as Raman scattering.³⁵ Moreover, the decrease in the peak

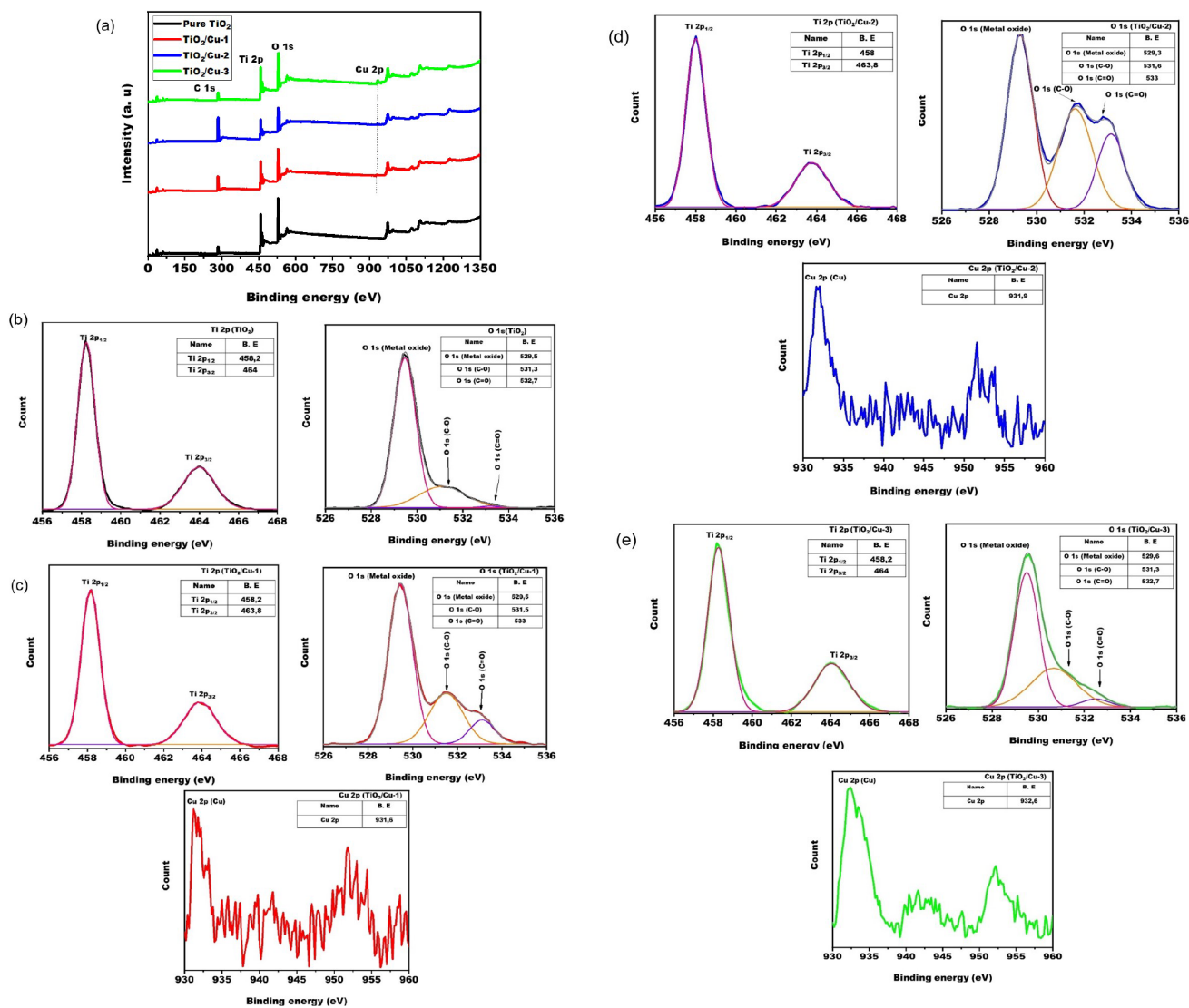


Figure 5. XPS spectra of TiO_2 and Cu-doped TiO_2 nanoparticles: (a) survey, (b) TiO_2 , (c) $\text{TiO}_2/\text{Cu-1}$, (d) $\text{TiO}_2/\text{Cu-2}$, and (e) $\text{TiO}_2/\text{Cu-3}$ [Ti 2p, O 1s, Cu 2p].

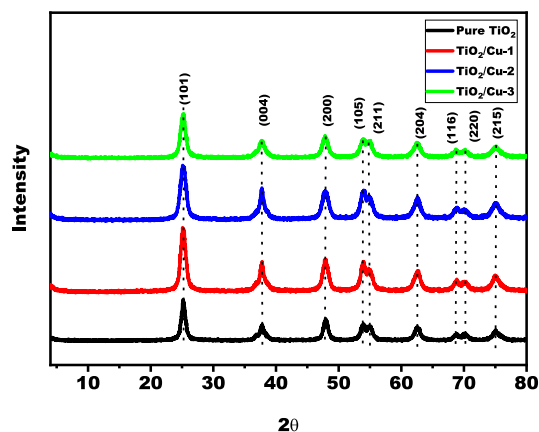


Figure 6. XRD patterns of TiO_2 and Cu-doped TiO_2 nanoparticles.

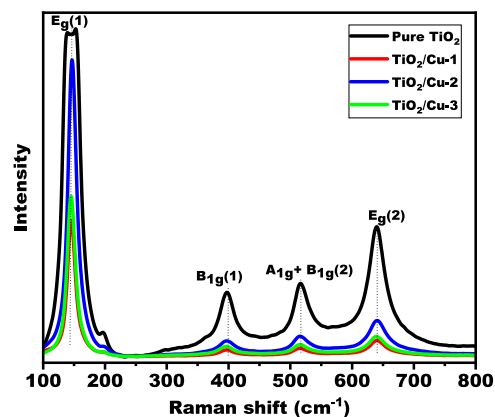


Figure 7. Raman spectra of TiO_2 and Cu-doped TiO_2 nanoparticles.

intensity could also be probably ascribed to the weakened O–Ti–O bond upon the addition of the Cu atoms.

3.7. Fourier-Transform Infrared Spectroscopy (FTIR) Analysis. Figure 8 shows the FTIR spectra of TiO_2 and $\text{TiO}_2/$

Cu nanoparticles. All the nanoparticles showed a characteristic peak at $3050\text{--}3600\text{ cm}^{-1}$ that corresponds to the stretching vibrations of the hydroxyl groups (O–H). The peaks at around 2300 and 2078 cm^{-1} correspond to CO_2 and C–O from the atmosphere. Meanwhile, the peak at around 1624 cm^{-1} is

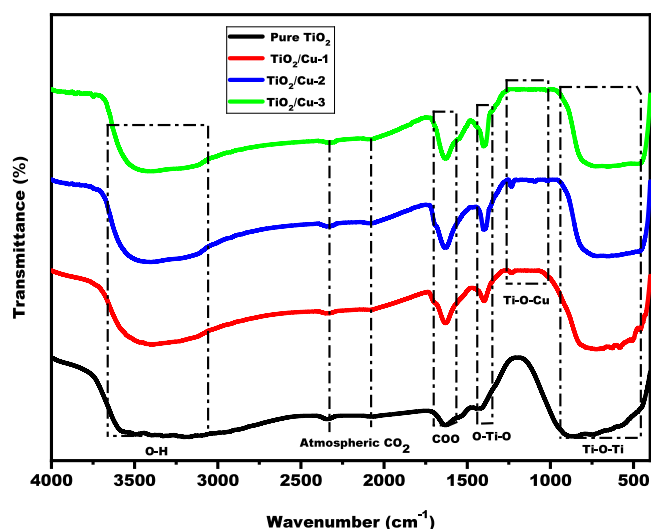


Figure 8. FTIR spectra of TiO_2 and Cu-doped TiO_2 nanoparticles.

attributed to the COO group and has been confirmed by Raguram and Rajni.³⁹ Moreover, the peaks at 1624 and 1400 cm^{-1} became more intense for the doped TiO_2 as compared to the pure TiO_2 nanoparticles. Maragatha et al.⁴⁰ showed that the peak at around 1400 cm^{-1} indicates stretching vibration of O–Ti–O, and the same peak is also observed in the current study which confirms the formation of TiO_2 . The peak at around 1200 cm^{-1} corresponds to Ti–O–Cu, which confirms the formation of the TiO_2/Cu nanoparticles. However, the peak is not visible in the $\text{TiO}_2/\text{Cu-3}$ sample; however, this has never been reported in the literature but may be assumed to be caused by the decrease in the number of Ti–O–Cu connections with an increase in Cu doping. Čizmar et al.⁴¹ reported where it was stated the number of Ti–O–Cu connections decrease with an increase in Cu concentration due to copper agglomeration on the TiO_2 surface. Chen et al.⁴² observed the same trend. The Ti–O–Cu peak intensity seems to be more prominent for $\text{TiO}_2/\text{Cu-2}$ as compared to the $\text{TiO}_2/\text{Cu-1}$ nanoparticles. Furthermore, a significant absorption band ranging from 400 to 1000 cm^{-1} corresponds to the vibration modes of Ti–O–Ti linkage in TiO_2 nanoparticles, which denotes the growth of the TiO_2 nanoparticles.^{39,43}

3.8. Thermogravimetric Analysis. Figure 9a presents the TGA thermogram of the fabricated nanoparticles, and Figure 9b–e represents the graphs for the derivative TGA of the nanoparticles. The TGA curves for the nanoparticles show three degradation steps. As for the pure TiO_2 nanoparticles (Figure 9b), the first degradation between 25 and 200 °C is accounted to the loss of residual organic solvent and physisorbed water with a mass loss of 1.8%.^{44,45} The second broad TGA exotherm peak in the range of 250–400 °C indicates decomposition of hydroxyl groups and organic molecules chemically bonded to the surface of the TiO_2 sample, giving a further mass loss of 2%.⁴⁶ Subsequent to that, insignificant weight loss occurred in the range of 400 to 800 °C due to the formation of high crystalline TiO_2 .^{47,48} The same trend was observed for the resultant Cu-doped TiO_2 nanoparticles (Figure 9c–e). The loss of residual organic solvent and physisorbed water appeared in the range of 25–100 °C with a mass loss of 4%, 5.4%, and 6.5% for $\text{TiO}_2/\text{Cu-1}$, $\text{TiO}_2/\text{Cu-2}$, and $\text{TiO}_2/\text{Cu-3}$, respectively. A TGA exotherm peak is also observed in the range of 250–400 °C depicting a

TGA mass loss of about 8%, due to the decomposition of hydroxyl groups and organic molecules. The formation of crystalline phase of the Cu-doped TiO_2 sample is characterized by no TGA exotherm peak in the temperature range of 540–900 °C. The results have shown that the addition of Cu in the TiO_2 matrix has patently affected the thermal property of TiO_2 . One can notice that the pure TiO_2 was more stable upon heating with smaller mass loss (5%) compared to $\text{TiO}_2/\text{Cu-1}$, $\text{TiO}_2/\text{Cu-2}$, and $\text{TiO}_2/\text{Cu-3}$ with mass loss of 8.2, 8.1, and 8.6, respectively. With that said, the thermal stability of TiO_2 has significantly decreased following the addition of Cu. This is assumed to be caused by a decrease in Ti–O–Cu interactions as observed in FTIR. The same trend was observed by Nankya et al.⁴⁹ and Rodríguez-Álvarez et al.⁵⁰

3.9. Brunauer–Emmett–Teller (BET) Analysis. Figure 10a–d presents the N_2 adsorption/desorption isotherms of TiO_2 and its resultant nanocomposites. As shown in the figure, the nitrogen adsorption/desorption of all the nanomaterials exhibited a type IV isotherm which relates to capillary condensation within mesopores.⁵¹ In accordance with the IUPAC classification, it occurs in mesoporous substances with cylindrical pores, along with H1 hysteresis loops.⁵² This isotherm develops with mesoporous adsorbents with pore radii varying from 25 to 500 Å.⁵³

Furthermore, the BET surface area, pore volume, and pore diameter were measured, and the results are illustrated in Table 3. It is seen that the surface area of the composites increased as the loading of Cu increased. However, both the pore volume and the pore diameter decreased upon incorporation of the Cu. These data are in agreement with both the XRD and the Raman spectroscopy analysis.

3.10. Antibacterial Evaluation of the Nanoparticles.

The antibacterial activity of TiO_2 and TiO_2/Cu nanoparticles was studied against two benign bacterial strains, *B. subtilis* and *E. coli* using the minimum inhibitory concentrations (MICs) and the minimum bactericidal concentrations (MBCs). The bacterial growth inhibition (%) and MIC values following treatment with the nanoparticles are presented in Figure 11 and Table 4, respectively. It is noticed that, all the nanoparticles had MIC values of 1.25 mg/mL against the Gram-positive *B. subtilis* and 2.5 mg/mL against the Gram-negative *E. coli*. The MICs against Gram-negative *E. coli* were higher as compared to Gram-positive *B. subtilis* as shown in Table 4. These results show that *B. subtilis* was more sensitive to treatment with the TiO_2/Cu nanoparticles compared to *E. coli*. The reasons for the higher inhibition efficacy of Gram-positive bacteria *B. subtilis* over Gram-negative *E. coli* are undetermined, but it could be due to the Gram-positive bacteria cell envelope's increased permeability toward cytotoxic Ti and Cu metal ions, which is made up of a cell membrane and a highly permeable cell wall. Although Gram-negative bacteria have a smaller cell envelope, it has two membrane layers with the outer being made up of primarily tightly bound lipopolysaccharide proteins that serve as effective penetration barriers.⁵⁴ This is also evident from the MIC₅₀ values obtained for each of these strains, where the MIC₅₀ values obtained for *B. subtilis* were ~1.6–2.7 folds lower than those obtained for *E. coli* (the lower the IC₅₀ value, the higher the biological activity). The potency of the Cu- TiO_2 nanoparticles against *B. subtilis* was in the order $\text{TiO}_2/\text{Cu-1} > \text{TiO}_2 > \text{TiO}_2/\text{Cu-2} > \text{TiO}_2/\text{Cu-3}$.

In terms of the antibacterial properties of the nanomaterials, the ability of the bacterial cells to regrow on the nutrient agar

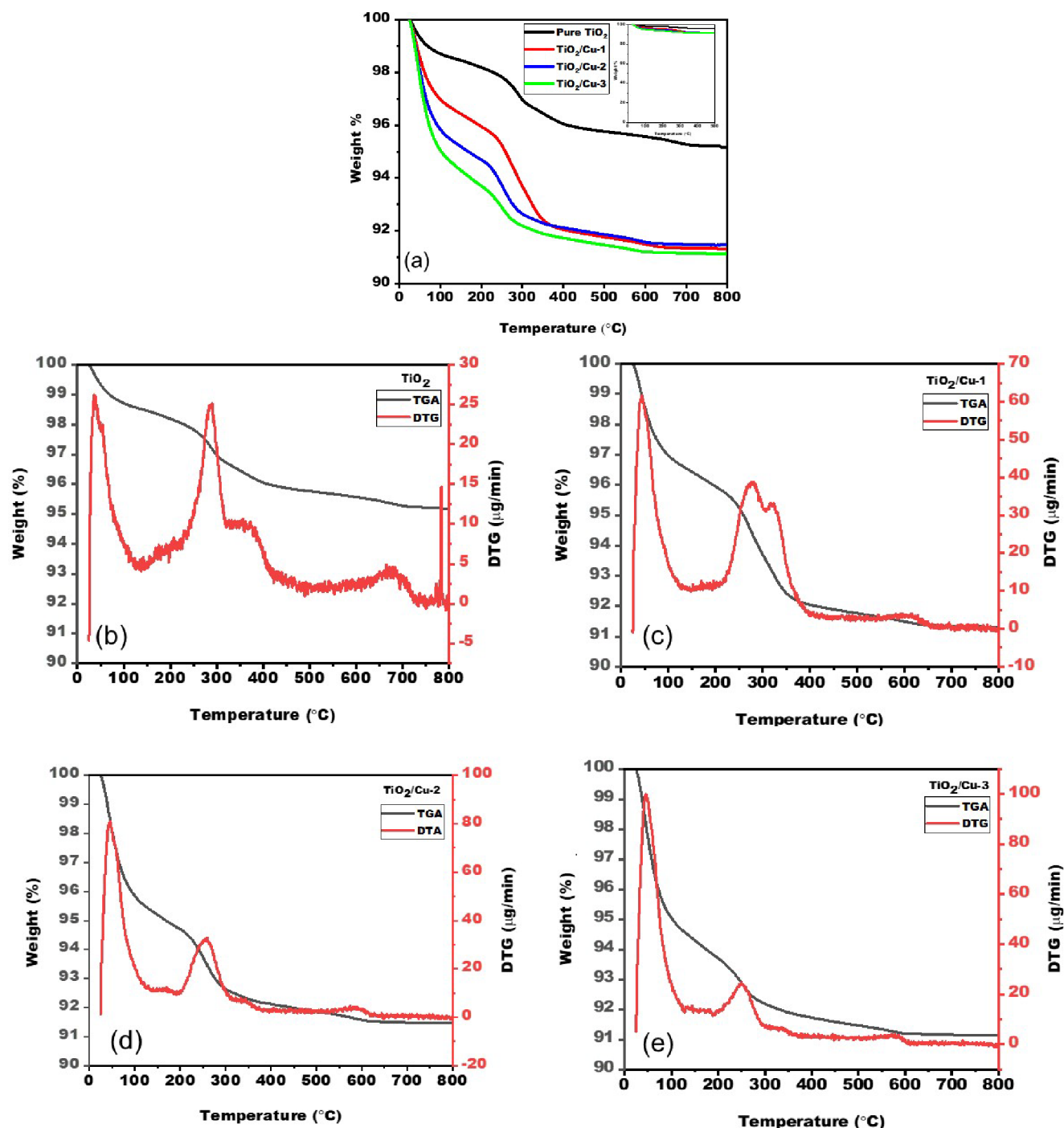


Figure 9. (a) TGA analysis of TiO₂ and TiO₂/Cu, and TGA-DTG of (b) TiO₂ and (c–e) TiO₂/Cu nanoparticles.

plates following their incubation on the MIC assay shows that the Cu-TiO₂ nanoparticles are bacteriostatic, and not bactericidal (i.e., they inhibit bacterial growth without killing the cells.^{55,56} The clinical importance of bactericidal and bacteriostatic samples, however, is still under dispute and is not used to rule out the potential application of samples as antimicrobial agents. In general, the results in Figure 11a,b have shown that no significant differences in the antimicrobial activity of the TiO₂ nanoparticles were observed in the presence and the absence of copper. Interestingly, the nanoparticles achieved 90 and 80% bacterial growth inhibition against *B. subtilis* and *E. coli* strains, respectively. Most

interestingly, high bacterial growth inhibition against both bacterial strains was achieved in the dark without any light source such as UV or visible light.

4. CONCLUSION

The TiO₂ and TiO₂/Cu nanomaterials were successfully prepared by the sol–gel method. The characterizations of the materials using various techniques confirmed the formation of nanoparticles with unique features. Moreover, a decrease in thermal stability of TiO₂ as the Cu loading increased was observed. The antimicrobial activity of the TiO₂ nanoparticles was not affected by the addition of Cu nanoparticles.

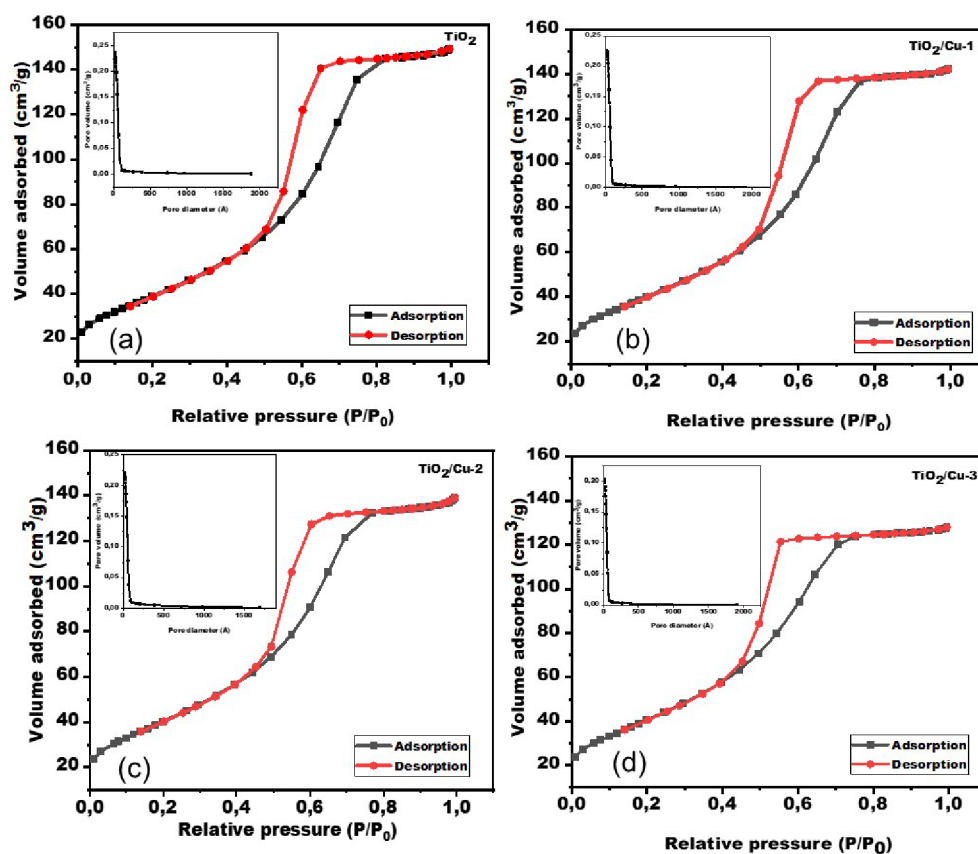


Figure 10. BET surface area analysis: N₂ adsorption–desorption isotherm (a) TiO₂ and (b–d) Cu-doped TiO₂ with BJH insets.

Table 3. Summary of BET Surface Area, Pore Volume, and Pore Diameter of TiO₂ and TiO₂/Cu

sample label	surface area (m ² /g)	pore volume (cm ³ /g)	pore diameter (Å)
Pure TiO ₂	145.999	0.227	62.296
TiO ₂ /Cu-1	149.078	0.217	58.193
TiO ₂ /Cu-2	151.459	0.210	55.472
TiO ₂ /Cu-3	152.695	0.195	51.151

Table 4. Summary of the MIC and MIC₅₀ of TiO₂ and TiO₂/Cu Against *B. subtilis* and *E. coli*

sample	MIC (mg/mL)		MIC ₅₀ (mg/mL)	
	<i>E. coli</i>	<i>B. Subtilis</i>	<i>B. Subtilis</i>	<i>E. coli</i>
TiO ₂	1.25	2.5	0.443	0.806
TiO ₂ /Cu-1	1.25	2.5	0.346	0.854
TiO ₂ /Cu-2	1.25	2.5	0.485	0.889
TiO ₂ /Cu-3	1.25	2.5	0.589	0.956

Interestingly, the bacterial growth inhibition of TiO₂ and TiO₂/Cu nanoparticles was nanoparticle's concentration dependent and found to be 90 and 80% against Gram-positive (*B. subtilis*) and Gram-negative (*E. coli*), respectively. These

findings show that the prepared nanoparticles have the potential to be used as antibacterial agents for water treatment due to their capability to inhibit bacterial growth in the dark without any light source.

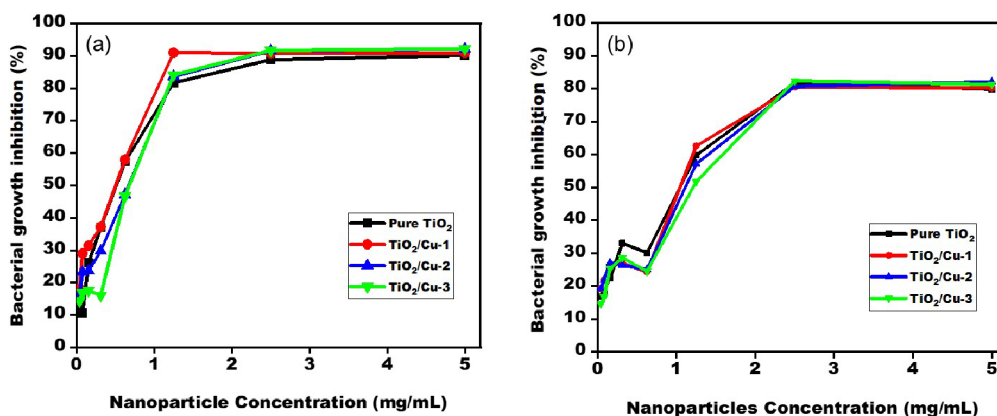


Figure 11. Antibacterial activity of TiO₂ and TiO₂/Cu against (a) *B. subtilis* and (b) *E. coli*.

AUTHOR INFORMATION

Corresponding Author

Thollwana Andretta Makhetha – Department of Chemical Sciences, University of Johannesburg, Doornfontein Campus, Johannesburg 2028, South Africa; DSI/Mintek Nanotechnology Innovation Centre, Water Research Node, University of Johannesburg, Doornfontein Campus, Johannesburg 2028, South Africa; orcid.org/0000-0003-1942-6661; Email: tamakhetha@uj.ac.za

Authors

Njabulo Sondezi – Department of Chemical Sciences, University of Johannesburg, Doornfontein Campus, Johannesburg 2028, South Africa; DSI/Mintek Nanotechnology Innovation Centre, Water Research Node, University of Johannesburg, Doornfontein Campus, Johannesburg 2028, South Africa

Zikhona Njengele-Tetyana – Advanced Materials Division, DSI/Mintek Nanotechnology Innovation Centre, Randburg 2125, South Africa

Kgabo Phillemon Matabola – Advanced Materials Division, DSI/Mintek Nanotechnology Innovation Centre, Randburg 2125, South Africa; Department of Water and Sanitation, University of Limpopo, Sovenga 0727, South Africa

Complete contact information is available at:

<https://pubs.acs.org/10.1021/acsomega.3c09308>

Notes

The authors declare no competing financial interest.

ACKNOWLEDGMENTS

The authors acknowledge the Department of Science and Innovation through the DSI/MINTEK Nanotechnology Innovation Centre (NIC) as well as DSI/NRF Thuthuka grant (TTK2204285229) for providing financial support during the course of the project.

REFERENCES

- (1) Singh Jassal, P.; Kaur, D.; Prasad, R.; Singh, J. Green synthesis of titanium dioxide nanoparticles: Development and applications. *J. Agric. Food Res.* **2022**, *10*, 100361.
- (2) Akhigbe, L.; Ouki, S.; Saroj, D. Disinfection and removal performance for *Escherichia coli* and heavy metals by silver-modified zeolite in a fixed bed column. *Chem. Eng. J.* **2016**, *295*, 92–98.
- (3) Gautam, S.; Agrawal, H.; Thakur, M.; Akbari, A.; Sharda, H.; Kaur, R.; Amini, M. Metal oxides and metal organic frameworks for the photocatalytic degradation: A review. *J. Environ. Chem. Eng.* **2020**, *8* (3), 103726.
- (4) Padmavathi, R.; Kalaivanan, C.; Raja, R.; Kalaiselvan, S. Antioxidant and antimicrobial studies of silver nanoparticles synthesized via chemical reduction technique. *Mater. Today Proc.* **2022**, *69*, 1339–1345.
- (5) Yadav, S.; Rani, N.; Saini, K. A review on transition metal oxides based nanocomposites, their synthesis techniques, different morphologies and potential applications. *IOP Conf Ser. Mater. Sci. Eng.* **2022**, *1225* (1), 012004.
- (6) Parashar, M.; Shukla, V. K.; Singh, R. Metal oxides nanoparticles via sol–gel method: a review on synthesis, characterization and applications. *J. Mater. Sci.: Mater. Electron.* **2020**, *31* (5), 3729–3749.
- (7) Atacan, K.; Güy, N.; Özmen, M.; Özacar, M. Fabrication of silver doped different metal oxide nanoparticles and evaluation of their antibacterial and catalytic applications. *Appl. Surf. Sci. Adv.* **2021**, *6*, 100156.
- (8) Kadiyala, U.; Kotov, N. A.; VanEpps, J. S. Antibacterial Metal Oxide Nanoparticles: Challenges in Interpreting the Literature. *Curr. Pharm. Des.* **2018**, *24* (8), 896–903.
- (9) Taman, R.; Ossman, M. E.; Mansour, M. S.; Farag, H. A. Metal Oxide Nano-particles as an Adsorbent for Removal of Heavy Metals. *J. Adv. Chem. Eng.* **2015**, *5* (3), 1000125.
- (10) Ramalingam, V.; Sundaramahalingam, S.; Rajaram, R. Size-dependent antimycobacterial activity of titanium oxide nanoparticles against: *Mycobacterium tuberculosis*. *J. Mater. Chem. B* **2019**, *7* (27), 4338–4346.
- (11) Abutalib, M. M.; Rajeh, A. Preparation and characterization of polyaniline/sodium alginate-doped TiO₂ nanoparticles with promising mechanical and electrical properties and antimicrobial activity for food packaging applications. *J. Mater. Sci.: Mater. Electron.* **2020**, *31* (12), 9430–9442.
- (12) Lee, H.; Jang, H. S.; Kim, N. Y.; Joo, J. B. Cu-doped TiO₂ hollow nanostructures for the enhanced photocatalysis under visible light conditions. *J. Ind. Eng. Chem.* **2021**, *99*, 352–363.
- (13) Sivaranjani, V.; Philominathan, P. Synthesize of Titanium dioxide nanoparticles using *Moringa oleifera* leaves and evaluation of wound healing activity. *Wound Med.* **2016**, *12*, 1–5.
- (14) Sathiyaseelan, A.; Saravanakumar, K.; Naveen, K.; Han, K.; Zhang, X.; Jeong, M.; Wang, M. Combination of Paraconiothryrium brasiliense fabricated titanium dioxide nanoparticle and antibiotics enhanced antibacterial and antibiofilm properties: A toxicity evaluation. *Environ. Res.* **2022**, *212*, 113237.
- (15) Erdem, A.; Metzler, D.; Cha, D.; Huang, C. P. Inhibition of bacteria by photocatalytic nano-TiO₂ particles in the absence of light. *Int. J. Environ. Sci. Technol.* **2015**, *12* (9), 2987–2996.
- (16) Gupta, K.; Joshi, P.; Gusain, R.; Khatri, O. P. Recent advances in adsorptive removal of heavy metal and metalloid ions by metal oxide-based nanomaterials. *Coord. Chem. Rev.* **2021**, *445*, 21410.
- (17) Wang, C.; Zhan, Y.; Wu, Y.; Shi, X.; Du, Y.; Luo, Y.; Deng, H. TiO₂/rectorite-trapped cellulose composite nanofibrous mats for multiple heavy metal adsorption. *Int. J. Biol. Macromol.* **2021**, *183*, 245–253.
- (18) Subhapiya, S.; Gomathipriya, P. Green synthesis of titanium dioxide (TiO₂) nanoparticles by *Trigonella foenum-graecum* extract and its antimicrobial properties. *Microb. Pathog.* **2018**, *116*, 215–220.
- (19) Amna, T.; Hassan, M.; Barakat, N.; Pandeya, D.; Hong, S.; Khil, M.; Kim, H. Antibacterial activity and interaction mechanism of electrospun zinc-doped titania nanofibers. *Appl. Microbiol. Biotechnol.* **2012**, *93* (2), 743–751.
- (20) Chen, S.; Guo, Y.; Chen, S.; Ge, Z.; Yang, H.; Tang, J. Fabrication of Cu/TiO₂ nanocomposite: Toward an enhanced antibacterial performance in the absence of light. *Mater. Lett.* **2012**, *83*, 154–157.
- (21) Leyland, N. S.; Podporska-Carroll, J.; Browne, J.; Hinder, S. J.; QUILTY, B.; Pillai, S. C. Highly Efficient F, Cu doped TiO₂ antibacterial visible light active photocatalytic coatings to combat hospital-acquired infections. *Sci. Rep.* **2016**, *6*, 24770.
- (22) Chen, S.; Guo, Y.; Zhong, H.; Chen, S.; Li, J.; Ge, Z.; Tang, J. Synergistic antibacterial mechanism and coating application of copper/titanium dioxide nanoparticles. *Chem. Eng. J.* **2014**, *256*, 238–246.
- (23) Preda, S.; Pande-Cuşu, J.; Petrescu, S.; Ciobanu, E.; Petcu, G.; Culiță, D.; Apostol, N.; Costescu, R.; Raut, I.; Constantin, M.; et al. Photocatalytic and Antibacterial Properties of Doped TiO₂ Nanopowders Synthesized by Sol–Gel Method. *Gels* **2022**, *8* (10), 673.
- (24) Fuentes, B.; Tapia, A.; Pozo, P. Synthesis, characterization, and antibacterial activity evaluation of Cu@TiO₂ nanocomposites. *Mater. Lett.* **2021**, *296*, 129885.
- (25) Mathew, S.; Ganguly, P.; Rhatigan, S.; Kumaravel, V.; Byrne, C.; Hinder, S.; Barlett, J.; Nolan, M.; Pillai, S. Cu-Doped TiO₂: Visible light assisted photocatalytic antimicrobial activity. *Appl. Sci.* **2018**, *8*, 2067.
- (26) Sagadevan, S.; Vinnila, S.; Singh, P.; Lett, J.; Oh, W.; Paiman, S.; Mohammed, F.; Al-Lohedan, H.; Fatimah, I.; Shahid, M.; et al.

- Exploration of the antibacterial capacity and ethanol sensing ability of Cu-TiO₂ nanoparticles. *J. Exp. Nanosci.* **2020**, *15* (1), 337–349.
- (27) Mushtaq, K.; Saeed, M.; Gul, W.; Munir, M.; Firdous, A.; Yousaf, T.; Khan, K.; Sarwar, H.; Riaz, M.; Zahid, S. Synthesis and characterization of TiO₂ via sol-gel method for efficient photocatalytic degradation of antibiotic ofloxacin. *Inorg. Nano-Met. Chem.* **2020**, *50* (7), 580–586.
- (28) Yadav, H. M.; Otari, S.; Koli, V.; Mali, S.; Hong, C.; Pawar, S.; Delekar, S. Preparation and characterization of copper-doped anatase TiO₂ nanoparticles with visible light photocatalytic antibacterial activity. *J. Photochem. Photobiol. A Chem.* **2014**, *280*, 32–38.
- (29) Wayan, P. *Clinical and Laboratory Standards Institute: Performance standards for antimicrobial susceptibility testing: 20th informational supplement*, 20th ed.; CLSI Document M100-S20, 2010.
- (30) Eloff, J. A sensitive and quick microplate method to determine the minimal inhibitory concentration of plant extracts for bacteria. *Planta Med.* **1998**, *64* (8), 711–713.
- (31) Challagulla, S.; Tarafder, K.; Ganesan, R.; Roy, S. Structure sensitive photocatalytic reduction of nitroarenes over TiO₂. *Sci. Rep.* **2017**, *7* (1), 8783.
- (32) Díez-Pascual, A. M. Antibacterial action of nanoparticle loaded nanocomposites based on graphene and its derivatives: A mini-review. *Int. J. Mol. Sci.* **2020**, *21* (10), 3563.
- (33) Raguram, T.; Rajni, K. S. Synthesis and characterisation of Cu-Doped TiO₂ nanoparticles for DSSC and photocatalytic applications. *Int. J. Hydrogen Energy* **2022**, *47* (7), 4674–4689.
- (34) Ślosarczyk, A.; Kłapiszewska, I.; Skowrońska, D.; Janczarek, M.; Jesionowski, T.; Kłapiszewski, Ł. A comprehensive review of building materials modified with metal and metal oxide nanoparticles against microbial multiplication and growth. *Chem. Eng. J.* **2023**, *466*, 143276.
- (35) Anitha, B.; Khadar, M. A. Dopant concentration dependent magnetism of Cu-doped TiO₂ nanocrystals. *J. Nanopart. Res.* **2016**, *18* (6), 149.
- (36) Pal, M.; Pal, U.; Jiménez, J.; Perez-Rodríguez, F. Effects of crystallization and dopant concentration on the emission behavior of TiO₂: Eu nanophosphors. *Nanoscale Res. Lett.* **2012**, *7* (1), 1–12.
- (37) Ahmadiasl, R.; Moussavi, G.; Shekoohiyan, S.; Razavian, F. Synthesis of Cu-Doped TiO₂ Nanocatalyst for the Enhanced Photocatalytic Degradation and Mineralization of Gabapentin under UVA/LED Irradiation: Characterization and Photocatalytic Activity. *Catalysts* **2022**, *12* (11), 1310.
- (38) Choudhury, B.; Choudhury, A.; Choudhury, A. Defect generation, d-d transition, and band gap reduction in Cu-doped TiO₂ nanoparticles. *Int. Nano Lett.* **2013**, *3* (1), 25.
- (39) Raguram, T.; Rajni, K. S. Synthesis and analysing the structural, optical, morphological, photocatalytic and magnetic properties of TiO₂ and doped (Ni and Cu) TiO₂ nanoparticles by sol-gel technique. *Appl. Phys. A: mater. Sci. Process.* **2019**, *125* (5), 1–11.
- (40) Maragatha, J.; Rajendran, S.; Endo, T.; Karuppuchamy, S. Microwave synthesis of metal doped TiO₂ for photocatalytic applications. *J. Mater. Sci.: Mater. Electron.* **2017**, *28* (7), 5281–5287.
- (41) čizmar, T.; Lavrenčič Štangar, U.; Fanetti, M.; Arčon, I. Effects of Different Copper Loadings on the Photocatalytic Activity of TiO₂-SiO₂ Prepared at a Low Temperature for the Oxidation of Organic Pollutants in Water. *ChemCatchem* **2018**, *10* (14), 2982–2993.
- (42) Chen, J. Y.; Yan, J. K.; Gan, G. Y. The Effect of Cu Doping on the Transformation from Rutile to Anatase and Cu Occupation Tendency in TiO₂ Solid Solution. *J. Spectrosc.* **2019**, *2019*, 6470601.
- (43) Rajamannan, B.; Mugundan, S.; Viruthagiri, G.; Praveen, P.; Shanmugam, N. Linear and nonlinear optical studies of bare and copper doped TiO₂ nanoparticles via sol gel technique. *Spectrochim. Acta, Part A* **2014**, *118*, 651–656.
- (44) Kite, S. V.; Sathe, D. J.; Kadam, A. N.; Chavan, S. S.; Garadkar, K. M. Highly efficient photodegradation of 4-nitrophenol over the nano-TiO₂ obtained from chemical bath deposition technique. *Res. Chem. Intermed.* **2020**, *46* (2), 1255–1282.
- (45) Tayel, A.; Ramadan, A. R.; El Seoud, O. A. Titanium dioxide/graphene and titanium dioxide/graphene oxide nanocomposites: Synthesis, characterization and photocatalytic applications for water decontamination. *Catalysts* **2018**, *8* (11), 491.
- (46) Bekele, E. T.; Gonfa, B. A.; Zelekew, O. A.; Belay, H. H.; Sabir, F. K. Synthesis of Titanium Oxide Nanoparticles Using Root Extract of *Kniphofia foliosa* as a Template, Characterization, and Its Application on Drug Resistance Bacteria. *J. Nanomater.* **2020**, *2020*, 1–10.
- (47) Alamgir; Khan, W.; Ahmad, S.; Ahammed, N.; Naqvi, A. H. Thermal analysis and temperature dependent dielectric responses of Co doped anatase TiO₂ nanoparticles. *AIP Conf Proc.* **2015**, *1661* (1), 080001.
- (48) Zuas, O.; Budiman, H. Synthesis of nanostructured copper-doped titania and its properties. *Nano-Micro Lett.* **2013**, *5* (1), 26–33.
- (49) Nankya, R.; Kim, K. N. Sol-gel synthesis and characterization of Cu-TiO₂ nanoparticles with enhanced optical and photocatalytic properties. *J. Nanosci. Nanotechnol.* **2016**, *16* (11), 11631–11634.
- (50) Rodríguez-Álvarez, A.; Silva-Martínez, S.; Pineda-Arellano, C. A. Influence of copper and iron transition metals in the photocatalytic activity of titanium dioxide microspheres. *J. Photochem. Photobiol. A Chem.* **2023**, *444*, 115016.
- (51) Kerrami, A.; Khezami, L.; Bououdina, M.; Mahtout, L.; Modwi, A.; Rhabi, S.; Bensouici, F.; Belkacemi, H. Efficient photodegradation of azucryl red by copper-doped TiO₂ nanoparticles—experimental and modeling studies. *Environ. Sci. Pollut. Res.* **2021**, *28*, 57543–57556.
- (52) Anupong, W.; On-Uma, R.; Jutamas, K.; Salmen, S.; Alharbi, S.; Joshi, D.; Jhanani, G. Antibacterial, antifungal, antidiabetic, and antioxidant activities potential of *Coleus aromaticus* synthesized titanium dioxide nanoparticles. *Environ. Res.* **2023**, *216*, 114714.
- (53) Alotaibi, A.; Williamson, B.; Sathasivam, S.; Kafizas, A.; Alqahtani, M.; Sotelo-Vazquez, C.; Buckeridge, J.; Wu, J.; Nair, S.; Scanlon, D.; et al. Enhanced Photocatalytic and Antibacterial Ability of Cu-Doped Anatase TiO₂ Thin Films: Theory and Experiment. *ACS Appl. Mater. Interfaces* **2020**, *12* (13), 15348–15361.
- (54) Bernatová, S.; Samek, O.; Pilát, Z.; Serý, M.; Ježek, J.; Jákl, P.; Siler, M.; Krzyžánek, V.; Zemánek, P.; Holá, V.; et al. Following the mechanisms of bacteriostatic versus bactericidal action using raman spectroscopy. *Molecules* **2013**, *18* (11), 13188–13199.
- (55) Carrapiço, A.; Martins, M. R.; Caldeira, A. T.; Mirão, J.; Dias, L. Biosynthesis of Metal and Metal Oxide Nanoparticles Using Microbial Cultures: Mechanisms, Antimicrobial Activity and Applications to Cultural Heritage. *Microorganisms* **2023**, *11* (2), 378.
- (56) Birhanu, R.; Afrasa, M. A.; Hone, F. G. Recent Progress of Advanced Metal-Oxide Nanocomposites for Effective and Low-Cost Antimicrobial Activates: A Review. *J. Nanomater.* **2023**, *2023*, 1–25.